Microstructures designed for shock robustness

Shawn Cunningham, David McIntyre[1], Judd Carper, Paul Jaramillo, and William Tang[2]

Ford Microelectronics, Inc., 9965 Federal Dr., Colorado Springs, CO, USA 80921

ABSTRACT

This research was performed to address the issue of shock robustness in silicon microstructures. The improvements were incorporated by considering features to reduce stress concentration and by geometries that have a more uniform stress distribution. The designs were evaluated by finite element models and by testing with wafer level techniques. The designs were intended to have the same fundamental frequency, inertia properties and damping properties. Six different designs were developed and distributed across 900 die on multiple 4-inch wafers. The wafers were subjected to repeated shocks at magnitudes of 130, 2008, and 3680 gs with a 0.25 msec duration.

Automated optical inspection was used to interrogate each die and determine which test structures survived the shock test. Subsequent to testing, analysis of variance was used to identify the significant factors that influence the failure rate. This analysis has shown beam design, wafer orientation, acceleration level, and the interactions of beam design*wafer orientation, wafer orientation*acceleration level to be significant factors contributing to the failure rate. The designs were grouped according to mean failure rate. The "small bow tie" design had the highest failure rate and was a separate population. Its failure rate was two to four times that of other designs. The second grouping of lower failure rates included all designs to address the stress concentration. Of these designs, the "no gusset" design has the highest failure rate (twice that of other designs). The final grouping includes the gusset designs and the "medium" and "large bow tie" designs. The designs to improve stress distribution had the lowest mean failure rates of all designs.

Keywords: shock, reliability, wafer level testing, silicon microstructures.

1. INTRODUCTION

For at least a decade, the focus of the MEMS (Micro Electro Mechanical Systems) community has been to develop novel processes and novel structures for sensors and actuators. The study of mechanical properties and computer aided engineering (CAE) for MEMS has been reported to a smaller extent. However, the commercial success of MEMS, in many areas, depends as much on quality and reliability as on novel processes or designs. The reliable product is developed with controlled processes, intelligent designs, applied CAE, and knowledge of material properties[1-5]. Automotive sensors must pass reliability tests[6] consisting of environmental stresses (e.g. thermal shock, thermal cycling, and moisture), electrical stresses, and mechanical stress (e.g. random vibration, swept sinewave, and handling drop). In addition, space applications[7] require an understanding of mechanical shock because of separation and deployment procedures and of potential damage caused by radiation.

A common qualification/verification test for automotive sensors is the handling drop. In this test, a fully functional sensor (including the sense element, ASIC, and package) is dropped from a specified height, tested for functionality, and evaluated for performance. This test will be in place for the qualification of a final sensor design; however, it is an expensive method for evaluating small process or design changes. A test of this nature would require a large number of parts to populate the experiment and make decisions with a high level of confidence. A large number of functional parts or packaged sense elements is an expensive means to populate the experiment. Another large expense is the failure analysis required to attribute the failure to the sense element, the ASIC, or the package (includes package body, leadframe, and bondwires). At the conclusion of the failure analysis, it can still be difficult to separate the failure of the sense element from a failure of the package. It was these difficulties that prompted the development of wafer level testing of microstructures for mechanical shock[8] and the pursuit of designs for shock robustness.

1. Currently with WinStar, Inc., Monument, CO 80132
2. Currently with Jet Propulsion Laboratory, Pasadena, CA 91109

0-8194-2278-9/96/$6.00

2. METHODOLOGY

The wafer level stress methodology[8] was developed to efficiently evaluate the effects of process and design changes. It is based on the fabrication of many test structures on a wafer, subjecting the wafer to different stresses, and performing an automated inspection. A wafer contains 900 die that total 1800 test structures. The test structures are designed to exhibit a certain set of characteristics, such as, vibration modes, damping, and inertia. For evaluation of a design variation, the desired designs can be patterned on the mask in an alternating array. The alternating array helps mitigate process variations on the structures. In this way many designs may be evaluated on a single wafer. A process step or sequence of steps could be evaluated by selecting a single test structure (one with a finite failure rate) and performing lot splits at the steps in question. The control for the experiment is the split that follows the normal process flow.

The test structure wafers are subjected to an initial automated optical screening following completion of the processing. This screening permits the calculation of failure rate through the process before any stress testing. Stress testing can include whole wafer temperature cycling, thermal shock, humidity variation, electrostatic shock, mechanical shock, or combinations of stresses. Automated optical inspection is performed to determine a failure rate for this level of stress. After the inspection, the stress-inspection process can be repeated to identify the effects of cumulative damage.

2.1. Shock testing

Shock characterization is performed on a hydraulic actuated shock table with a mechanical amplifier to achieve higher shock magnitudes. Shock amplitudes of 30,000 gs for 0.1 msec can be investigated in this configuration. Two wafer mounts have been designed to hold the wafers on the shock table and achieve multiple loading modes simultaneously. The left mount in Fig. 1 will be referred to as the vertical mount. It orients the wafers parallel to the shock input. In this orientation, the layout of the structures allows the simultaneous testing of two different loading modes. The horizontal mount is shown on the right in Fig. 1. It is capable of holding two wafers: One facing the shock table (horizontal lower, HL) and one facing away from the shock table (horizontal upper, HU). The two structures in each die will observe the same shock which effectively doubles the number of test die on the wafer. A recession is machined into each mount to accommodate 4-inch wafers. The recession includes a flat to match the wafer flat and maintains the wafer orientation.

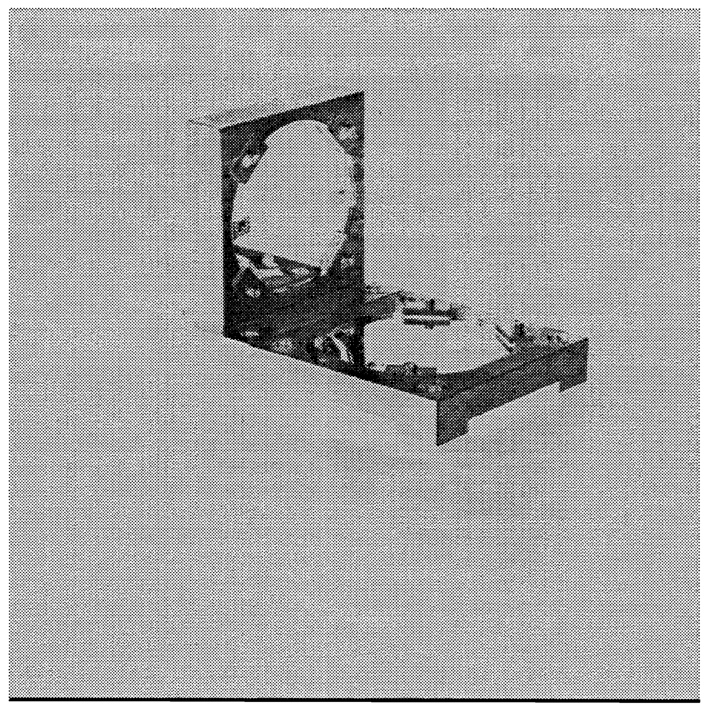

Figure 1. Wafer Mounts. The left mount supports the wafer in a vertical position and the horizontal mount, on the right, supports the wafer in the horizontal position.

Once the wafers are placed in the mounts and the mounts fixed to the shock table, a shock of specified magnitude and duration is applied. Shock magnitudes of 130, 2008, and 3680 gs and 0.25 msec duration were applied to different sets of wafers. The magnitude and duration is verified by a reference accelerometer fixed to the mounts. Shock testing was continued up to 100 shocks for most wafers; however, testing of some wafers was discontinued because of a substrate failure. Between each sequence of shocks, visual inspection of the wafer was performed to determine an incremental failure rate for the structures.

2.2. Automated Visual Inspection

Automated visual inspection was used to reduce the inspection time and improve the reliability of the output (in contrast to manual inspection performed by one or more persons). It was performed on a View Bazic 8 inspection system. Prealignment of the wafer is critical to obtain a 1 micron alignment accuracy between the machine coordinate system and the wafer coordinate system. First the sample stage is located relative to the inspection stage using custom hardware. This prealignment is used to capture a minimum of two alignment targets on the wafer. Once aligned, the inspection proceeds on a die by die basis.

The test structure handling wafer was designed specifically to aid the automated optical inspection. The silicon test structures are bonded to transparent pyrex for handling. The pyrex surface to which the structure is bonded is coated with a thin film of evaporated chrome. The chrome is patterned such that pyrex is exposed at the regions where the pedestals are bonded and directly beneath the test structure proof mass and beams. The metallization blocks transmitted light except beneath the proof mass.

Each die is inspected to determine the presence or absence of the proof mass. The die inspection begins by illuminating a pedestal from above to focus the image. Next, the proof mass location is illuminated by transmitted light under precise intensity control. A pixel count is made at the center of the image and compared to a predetermined threshold pixel count. An intensity distribution below the threshold and a dark image indicate the presence of the test structure. The absence of a test structure is indicated by a bright image and the intensity distribution above the threshold. The binary information for each die is stored in an electronic wafer map for future statistical analysis.

3. TEST STRUCTURE FABRICATION

The basic sequences of the test structure fabrication are an anisotropic wet etching to form the test structure, a dissolved wafer process to release the test structure, and anodic bonding of silicon to pyrex for handling the test structures. A (100) n- silicon wafer with a p+ etch stop layer and a n- epitaxial layer is the starting point of the process as shown by Fig. 3 (a). The first step to define the test structures is the pedestal etch which typically defines a 4.5 μm gap. Figure 3 (b) shows the completed pedestals that have been masked by Si_3N_4 and etched in KOH. The pedestals have two important functions. First, the pedestal is anodically bonded to the pyrex substrate and supports the freely suspended test structure. Second, the pedestal etch defines the gap between the test structure and the substrate which controls the damping in all loading modes. In Fig. 3 (c), the test structure is shown as it is masked by Si_3N_4 after being etched in KOH. The completed test structure (including mass and beams) is typically 6.4 μm thick.

Once the nitride mask is removed from the completed test structures, the test structures are anodically bonded to a pyrex wafer. The pyrex wafer acts as a handling wafer during subsequent processing, testing and measurement. The advantages of the pyrex wafers have been described. The limitation of pyrex wafers is it can not withstand shocks as high a silicon. The test structure wafer is shown bonded to the pyrex wafer in Fig. 3 (d).

The dissolved wafer process is completed by removing the n- silicon handling wafer, as shown in Fig. 3 (e), and by the removal of the p+ silicon etch stop layer, as shown in Fig. 3 (f). The freely supported test structures are suspended from the pedestal. At the conclusion of the fabrication, the wafers are subjected to an after process automated visual inspection to identify all structures that did not complete the process.

4. TEST STRUCTURE DESIGN

The test structures have been designed to study the ability of design to effect the failure rate caused by shock loading. A test structure die is shown in Fig. 4. It shows two proof masses that are each suspended by two beams from the square pedestals. The entire die is covered by evaporated chrome except beneath the test structure (as can be seen beneath the beams). For each design, the torsional spring constant about the long axis of the beams is maintained at an approximately constant value. Other constants are the beam length, the damping, and the inertia properties. Two parameters that do change with design are the in-plane and out-of-plane bending stiffness.

Two test structures per die has advantages. First, a wafer placed in the horizontal holder (loading perpendicular to the substrate) has twice as many samples being tested because both structures in the die are subjected to the same input conditions. If the wafer is placed in the vertical holder, it is possible to test two different loading modes simultaneously, which provides a means for direct comparison.

The beam designs were developed by following the properties[9] of structures with shock/impact integrity. The first property is concerned with the selection of materials, which will not be considered because this study is constrained to single crystal silicon. It recommends using materials with a low elastic modulus and high strength. The second property is a large volume because more material volume is available to distribute the total strain energy. The final property is a uniform distribution of stress which uses the available material more effectively. The following discussion will implement these ideas to develop a more uniform stress distribution for improved shock robustness.

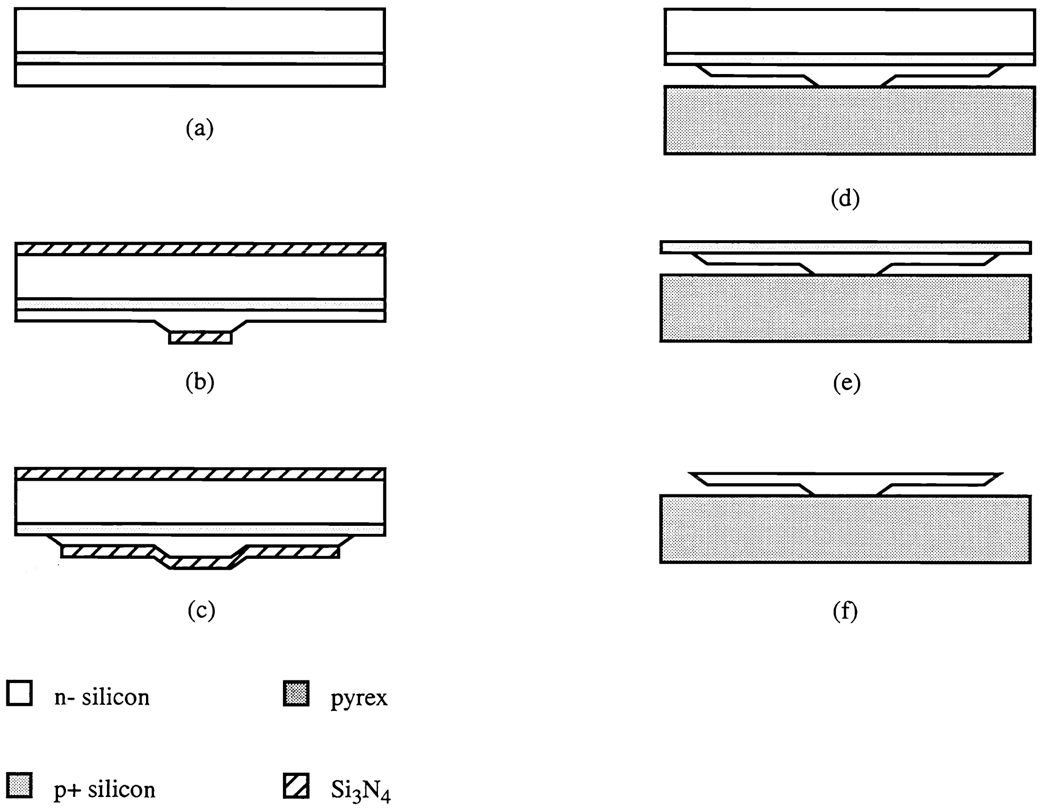

Figure 3. Process for fabrication of shock test structures. (a) npn starting wafer, (b) masked wafer following pedestal etch, (c) masked wafer following the completed etch of the test structure, (d) completed test structure shown anodically bonded to pyrex wafer, (e) bonded structure with the n- silicon handling wafer dissolved, (f) bonded test structure with the p+ silicon etch stop removed.

4.1. The ideal stress distribution

The test structure deformation shown in Fig. 5 will be used as the example to develop the background of the design changes. It shows a mass that has translated parallel to the substrate which deforms the beams. As shown in Fig. 5, the pedestal end of the beam behaves with fixed boundary conditions (zero displacement and zero curvature). The mass end translates (nonzero displacement), but is constrained to have zero curvature. For the bending conditions outlined, the bending moment varies linearly along the length of the beam and is a symmetric distribution with a maximum at either end. The stress distribution of this beam has the linear distribution shown in Fig. 6, because the bending moment has a linear distribution too. The stress distribution is the same for out-of-plane bending also. The stress has been normalized to the maximum stress at either end of the beam. The length has been normalized by the total length of the beam. The maximum bending stress in a beam is described by Eq. 1 where $\sigma(x)$ is the stress, $M(x)$ is the bending moment along the length of the beam, c is the distance from the beam's neutral axis to the point of interest, I is the area moment of inertia,

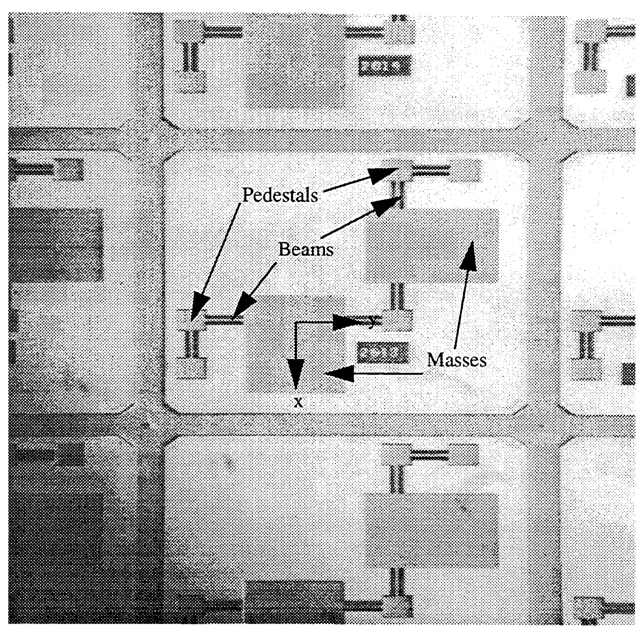

Figure 4. A test structure die that shows two proof masses each suspended by two beams from the pedestals.

and x is the distance along the length of the beam. In many designs, I and c are not a function of x but are independent of the distance along the beam.

$$\sigma(x) = \frac{M(x) \cdot c}{I} \tag{1}$$

The stress can be distributed uniformly by the appropriate design of I or c. Two beam views from Fig. 7 will be considered. It shows a beam (7 (a)) with a constant width and thickness (as analyzed in Fig. 6). The second beam (7 (b)) has a constant thickness and a width that varies linearly along a portion of the length. The constant cross-section beam has an area moment of inertia that is constant along its length and given by $I_c = w\ t^3/12$ for out-of-plane bending. Similarly, the variable cross-section beam has an area moment of inertia that varies linearly along a portion of its length. It is given by $I_v = w(x)\ t^3/12$. The variable moment of inertia is produced by a linear variation in the beam width. This is intended to improve the stress distribution near the ends where it is largest. It is obvious that the width can not decrease to zero near the beam's midpoint, therefore, a short constant width region remains. This design does not develop uniform stress in all modes but does reduce the stress near the ends because I is larger and increases faster than c increases. The thickness is not varied because of the limitations of the fabrication process.

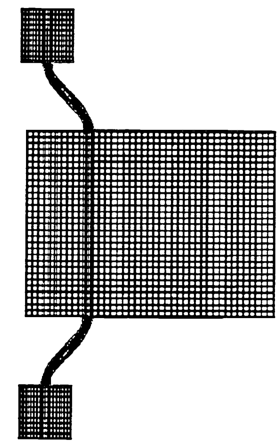

Figure 5. Deformation plot for test structure translation parallel to the substrate.

In this experiment, six beam designs will be considered for improved shock response. The details of the designs are shown in Fig. 7. All beams are 6.4 μm thick with the characteristic trapezoidal cross-section that results from anisotropic etching. Three beam designs address the issue of stress concentration by implementing two gusset designs. Figure 7(a) shows a straight beam with right angles at the ends. Figures 7 (b) and (c) show two gusset designs that have been implemented to reduce the stress concentration. The final three designs address the issue of developing a more uniform stress distribution. According to the previous discussion, the more uniform stress distribution would be developed by varying the moment of inertia. Figures 7 (d), (e), and (f) show the variable inertia beams which were accomplished by a linear variation of the beam width. Ideally, the beam width should approach zero at the beam's midpoint to completely compensate for the bending moment distribution, but this is not a realistic solution. This problem was approached by using a variable width near the ends of the beam and a constant width near the mid-section of the beam. As a result, the stress distribution should be more uniform near the ends of the beam where the stress is highest.

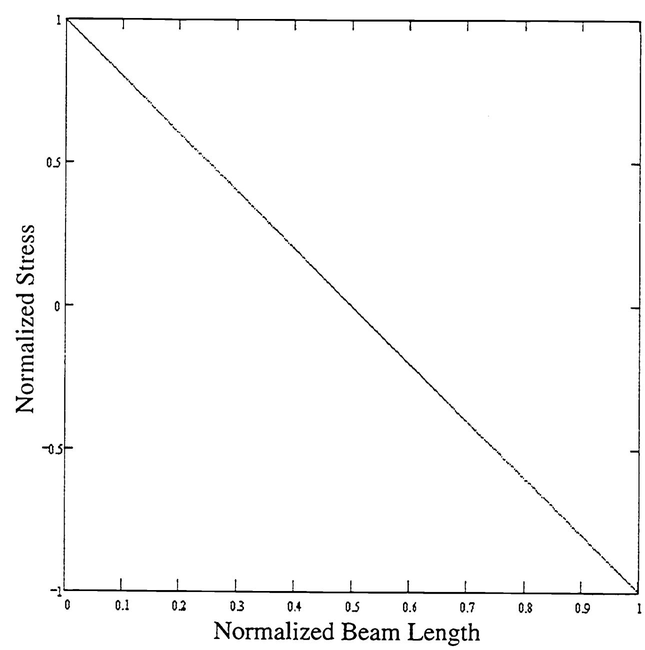

Figure 6. Normalized stress distribution along length of beam deformed as shown in Fig. 5.

4.2. Finite element models of stress distribution

Finite element models of the designs have been developed to better understand any improvements. Three different loading modes were modeled for each beam. In one loading mode, the shock load is applied along the x-axis as shown in Fig. 4, which causes the mass to translate along the x-axis. If the loading is applied along the y-axis, the same test structure will rotate in-plane in a yawing motion. It can be seen that for loading in either direction both modes will be excited because of the orthogonal layout of two test structures. The first two loading modes produce bending stresses in the two beams. The third loading is applied along the z-axis and perpendicular to the wafer. This causes the test structure to both rotate about the beam axis (y-axis as drawn) and translate along the z-axis. The resulting stress distribution is a superposition of the bending stress and torsion stress.

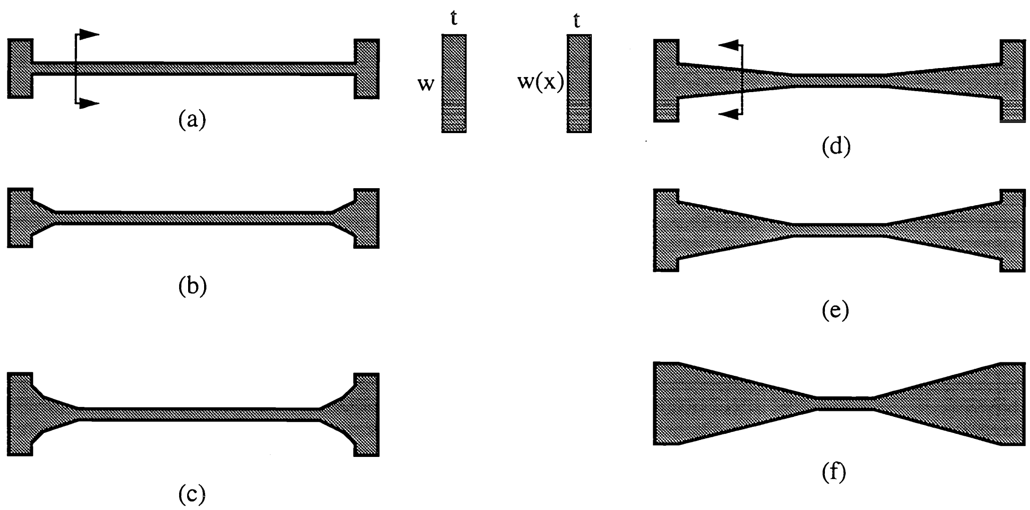

Figure 7. Beam designs to improve shock robustness. (a) "no gusset" design, (b) "Simple gusset" design, (c) "Compound gusset" design, (d) "Medium bow tie" design, (e) "Large bow tie" design, and (f) "Small bow tie" design.

4.3. Lumped parameter modeling of shock response

The shock test structures can be modeled in a simple way as a lumped parameter system consisting of a mass, a spring, and a damper as shown if Fig. 8. The lumped model is developed by reducing the continuum model to the three parameters. A separate lumped parameter model has been developed for each of the vibration modes tested. These modes include the pure translation parallel to the substrate, a rotation parallel to the substrate, and a combined rotation and translation perpendicular to the plane of the substrate.

The mass properties are simple to analyze for the rectangular proof mass. The mass is calculated for the translation modes. The mass moment of inertia is calculated for rotation about the different axes. The spring constant is calculated by using simple beam theory to determine the translational and angular deflection. The damping in the structures consists of two different varieties shown in Fig. 9. Figure 9 (a) shows a flat plate moving perpendicular to a substrate. This motion produces a pumping action that forces fluid out during the compression motion and forces the fluid in during the pulling motion. This is referred to as squeeze film damping[10] and is present during the motion perpendicular to the substrate. In Fig. 9 (b), a damping model is shown for motion parallel to the substrate. It consists of a model of Couette flow between the sub-

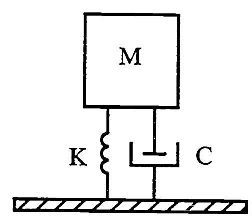

Figure 8. A lumped parameter system model for the shock test structures consisting of a mass, M, a spring, K, and a viscous damper, C.

strate and plate and Stokes flow between the plate and the stationary fluid above the plate.[12,13].

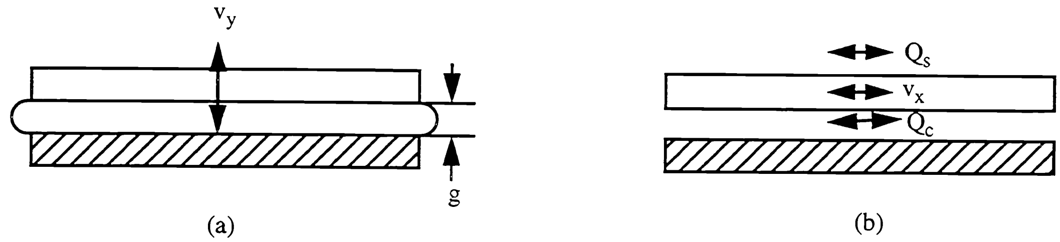

Figure 9. Damping models for the shock microstructures. (a) Squeeze film damping for motion perpendicular to the plane of the substrate. (b) Couette and Stokes flow damping for motion parallel to the plane of the substrate.

5. EXPERIMENTAL RESULTS

5.1 Experimental design

The experiment is designed to compare six beam designs for improved shock robustness. The details of the beams are shown in Fig. 7. All beams are 6.7 microns thick and 250 microns long with the characteristic trapezoidal cross-section that results from anisotropic etching. The qualitative reference for the "bow tie" beam designs refers to the dimension of the constant width section of the beam. The "small bow tie" design has a mid section of only 4 microns. It has tapered sections 77.5 microns long by 135 microns at the wide end. The "medium bow tie" design has a midsection width of 5 microns, a length of 110.5 for the variable widthsection and a major width of 38 microns. The "large bow tie" design has the widest midsection at 7microns. Its variable width section has a length of 110.5 microns and a major width of 32 microns. The minimum width of the "bow tie" designs is compared to the "no gusset" design with a width of 15 microns.

The six designs were fabricated in an array on the same wafer so that all designs could be tested simultaneously. The wafers were subjected to 100 drops at 130, 2008,or 3680 gs with durations of 0.25 msec. Individual wafers were tested in the vertical mount and in the horizontal mount with the test structures facing away from the shock table. The cumulative failure rate will be examined as a function of acceleration level, orientation, and beam design. This will determine which factors are significant for the design and which designs are a separate improved population.

5.2. Experimental results

This experimental design included several different variables including beam design (DESIGN), wafer orientation (WORIENT), acceleration level (GLEVEL), and beam orientation (BORIENT). In order to determine the significance of each variable, analysis of variance (ANOVA) has been performed on the cumulative failure rate data. The summary of the ANOVA results are shown in Table 1. In Table 1, the source column lists the experimental variables (DESIGN, WORIENT, GLEVEL, and BORIENT), and six, two-way interaction terms (DESIGN*WORIENT, DESIGN*GLEVEL, DESIGNN*BORIENT, WORIENT*GLEVEL, WORIENT*BORIENT, AND GLEVEL*BORIENT). The second column shows the number of degrees of freedom associated with each source. The mean square is an indicator of the variance associated with the corresponding source. The F-Value and Pr>F are indicators of the statistical significance of the corresponding source. These tests indicate DESIGN, WORIENT, GLEVEL, DESIGN*WORIENT, AND WORIENT*GLEVEL are significant at an alpha of 0.05 (Type I error).

The purpose of this experiment was to develop beam designs that are more robust to shock. The comparison between the failure rate of different designs is shown in Table 2. It was developed from Duncan's multiple range test for failure rate. This test groups together means that are not significantly different This test shows the small bow tie design is a separate population with the highest failure rate (approximately 2 to 4 times higher than other designs). The next grouping include all designs that address the issue of stress concentration. Although the "no gusset" design has a failure rate twice that of the gusset designs, they can not be distinguished as separate populations. The third grouping includes the gusset designs and the designs for improved distribution of stress. It is evident that the lowest failure rate is associated with the improved distribution of stress. The difference in designs could be emphasized by retesting with a single wafer orientation and acceleration level. A final point should be made with regard to the small bow tie result. Without regard to modeling and experimentation, the structure can be overcompensated and increased failures observed

	R^2	Root MSE	Failrate Mean	
	0.881	0.0771	0.0923	
Source	DF	Mean Square	F-Value	Pr>F
DESIGN	5	0.07993	13.46	0.0001
WORIENT	1	0.2356	39.66	0.0001
GLEVEL	2	0.1210	20.37	0.0001
BORIENT	1	0.01380	2.32	0.1359
DESIGN*WORIENT	5	0.0755	12.71	0.0001
DESIGN*GLEVEL	10	0.01644	2.77	0.0117
DESIGN*BORIENT	5	0.001677	0.28	0.9198
WORIENT*GLEVEL	2	0.08329	14.02	0.0001
WORIENT*BORIENT	1	0.005586	0.94	0.3385
GLEVEL*BORIENT	2	0.008730	1.47	0.2431

Table 1: ANOVA results for experimental variables and interactions.

Design	Failrate Mean	Duncan Grouping
Small Bow Tie	0.24714	A
No Gusset	0.11953	B
Standard Gusset	0.05319	BC
Compound Gusset	0.05316	BC
Medium Bow Tie	0.04907	C
Large Bow Tie	0.03182	C

Table 2: Duncan's multiple range test for failure rate of beam designs

6. ACKNOWLEDGMENTS

Monika Everett is recognized for performing the mask layouts for the test structures. The careful fabrication of the structures was completed by Ruth Wendlowsky, Sang Ko, and Connie Sweney. Joe Petersen, of Hauser Labs, Boulder CO, was helpful in developing these testing methods.

7. REFERENCES

1. S. J. Cunningham, W. Suwito, and D. T. Read, "Tensile testing of epitaxial silicon films," *Proc. 8th Int. Conf. Solid-State Sensors and Actuators, Transducers 95*, pp. 96-99, Stockholm, Sweden, 1995.
2. G. L. Pearson, W. T. Read, and W. L. Feldman, "Deformation and fracture of small silicon crystals," *Acta Metallurgica*, Vol. 5, pp. 181-191, 1957.
3. X. Ding, W. Ko, and J. M. Mansour, "Residual stress and mechanical properties of boron-doped p+ silicon films," *Sensors and Actuators*, A21-A23, pp. 866-871, 1990.
4. S. Johansson, F. Ericson, and J. -A. Schweitz, "Influence of surface coatings on elasticity, residual stress, and fracture properties of silicon microelements," *J. Appl. Physics*, Vol. 65, No. 1, pp. 122-128, 1989.
5. F. Ericson and J. -A. Schweitz, "Micromechanical fracture strength of silicon," *J. Appl. Physics*, Vol. 68, No. 11, pp. 5840-5844, 1990.
6. J. M. Giachino, "Automotive sensors: Driving toward optimized vehicle performance,"*7th Int. Conf. Sensors and Actuators, Tranducers '93*, pp. 982-987, Yokohama, Japan, 1993.
7. L. Muller, M. H. Hecht, L. M. Miller, H. K. Rockstad, and J. C. Lyke, "Packaging and qualification of MEMS-based space systems, *Proc. IEEE 9th Int. Workshop Micro Electro Mechanical Systems*, pp. 503-508, San Diego, CA, USA, 1996.
8. D. G. McIntyre, S. J. Cunningham, J. S. Carper, P. D. Jaramillo, and W. C. Tang, "A methodologyto study wafer level response of silicon microstructures to mechanical shock," to be published at ICME 1996, Atlanta, GA.
9. F. P. Beer and E. R. Johnston, Jr., *Mechanics of Materials,* Chapter 10, McGraw-Hill, New York, 1981.
10. J. B. Starr, "Squeeze-film damping in solid-state accelerometers," *IEEE Solid-State Sensor and Actuator Workshop*, pp. 44-47, Hilton Head, SC, USA, 1990.
11. X. Zhang and W. C. Tang, "Viscous air damping in laterally driven microresonators," *Sensors and Materials*, Vol. 7., No. 6, pp. 415-430, 1995.
12. Y. -H. Cho, B. M. Kwak, A. P. Pisano, and R. T. Howe, "Slide film damping in laterally driven microstructures," *Sensors and Actuators A*, 40, pp. 31-39, 1994.